

Direct Observation of the Superfluid Phase Transition in Ultracold Fermi Gases

Martin W. Zwierlein, Christian H. Schunck, André Schirotzek, and Wolfgang Ketterle

¹*Department of Physics, MIT-Harvard Center for Ultracold Atoms, and Research Laboratory of Electronics, MIT, Cambridge, MA 02139*

Water freezes into ice, atomic spins spontaneously align in a magnet, liquid helium becomes superfluid: Phase transitions are dramatic phenomena. However, despite the drastic change in the system's behaviour, observing the transition can sometimes be subtle. The hallmark of Bose-Einstein condensation (BEC) and superfluidity in trapped, weakly interacting Bose gases is the sudden appearance of a dense central core inside a thermal cloud ¹⁻⁷. In strongly interacting gases, such as the recently observed fermionic superfluids ⁸, this clear separation between the superfluid and the normal parts of the cloud is no longer given. Condensates of fermion pairs could be detected only using magnetic field sweeps ⁹⁻¹¹ into the weakly interacting regime. The quantitative description of these sweeps presents a major theoretical challenge. Here we demonstrate that the superfluid phase transition can be directly observed by sudden changes in the shape of the clouds, in complete analogy to the case of weakly interacting Bose gases. By preparing unequal mixtures of the two spin components involved in the pairing ^{12,13}, we greatly enhance the contrast between the superfluid core and the normal component. Furthermore, the non-interacting wings of excess atoms serve as a direct and reliable thermometer. Even in the normal state, strong interactions significantly deform the density profile of the majority spin component. We show that it is these interactions which drive the normal-to-superfluid transition at the critical population imbalance of 70(5)% ¹².

The dramatic signature of BEC in weakly interacting gases in atom traps derives from a natural hierarchy of energy scales: The critical temperature for condensation $T_C \propto n^{2/3}$ at particle density n is much larger than the chemical potential (divided by the Boltzmann constant k_B) of a pure condensate, $\mu \propto na$, which measures the interaction strength between atoms (a is the scattering length). Hence, for weak (repulsive) interactions ($na^3 \ll 1$), the condensate is clearly distinguished from the cloud of uncondensed atoms through its smaller size and higher density. However, as the interactions are increased, for example by tuning a using a Feshbach resonance, this hierarchy of energy scales breaks down, as μ can now become comparable to $k_B T_C$. In Fermi gases with weak attractive interaction ($a < 0$), $\mu \propto E_F$ will even exceed $k_B T_C \propto E_F \exp^{-\pi/2k_F|a|}$ by far ($E_F = \hbar^2 k_F^2 / 2m$ is the Fermi energy). Both the normal and the condensed cloud will here be of the same size given by the Fermi Radius $R_F \propto \sqrt{E_F}$.

The phase transition from the normal to the superfluid state, although dramatic in its consequences, is thus not revealed by a major change in the appearance of the gas. Indeed, in strongly interacting Fermi gases no deviation from a normal cloud's shape could so far be detected; neither in the unitary regime, where a diverges, nor on the attractive (BCS-)side of a Feshbach resonance. Theoretical works predicted small "kinks" ¹⁴⁻¹⁶ or other slight deviations ¹⁷ in the density profiles

of the gas in the superfluid regime, but after line-of-sight integration these effects have so far been too small to be observable. Condensates could only be observed via rapid magnetic field ramps to the BEC-side ($a > 0$) of the Feshbach resonance, performed during expansion^{9,10}. This suddenly reduced the condensate's chemical potential and let the thermal fraction grow beyond the condensate size. A similar ramp was used to detect vortices on resonance and on the BCS-side in the demonstration of fermionic superfluidity⁸. However, these magnetic field ramps are difficult to model theoretically, and a satisfactory quantitative comparison of e.g. the condensate fraction with experiments has not been accomplished^{18–21}.

In this work we demonstrate that the normal-to-superfluid phase transition in a strongly interacting Fermi gas can be directly observed from absorption profiles, without the need of any magnetic field ramps. As in the case of weakly interacting BECs, preparation, expansion and detection of the sample all take place at the same, fixed magnetic field and scattering length. As for BECs, the phase transition is observed by a sudden change in the shape of the cloud during time-of-flight expansion, when the trap depth is decreased below a critical value. To clearly distinguish the superfluid from the normal component we break the number symmetry between spin up (majority atom number N_{\uparrow}) and spin down (minority atom number N_{\downarrow}) and produce an unequal mixture of fermions (imbalance parameter $\delta = (N_{\uparrow} - N_{\downarrow}) / (N_{\uparrow} + N_{\downarrow})$). Standard BCS superfluidity requires equal densities of the two spin components. Hence, when cooled below the phase transition the cloud should show a sudden onset of a superfluid region of equal densities. Indeed, below a critical temperature, we observe a bimodal density distribution of the smaller cloud.

Breaking the symmetry in atom numbers thus produces a direct and striking signature of the superfluid phase transition. A similar situation has been encountered in Bose-Einstein condensation, where breaking the symmetry of a spherical trap resulted in dramatic anisotropic expansion of the condensate, now a hallmark of the BEC phase transition.

Fig. 1 shows column density profiles of the two imbalanced spin states for different points along the evaporation path corresponding to different temperatures, and for three magnetic fields corresponding to the BEC-side, exact resonance and the BCS-side of the resonance. For high final trap depths (upper panels in Fig. 1), the smaller cloud has the expected shape of a normal, non-superfluid gas: It is very well fit using a single, finite temperature Thomas-Fermi-profile (with central optical density, radius and the fugacity as independent fit-parameters). However, below a critical trap depth, a second, denser feature appears in the center of the minority component (lower panels in Fig. 1). This onset of bimodality occurs very suddenly as the trap depth is lowered, as can be seen from Fig. 2: Around the critical point, the atom number (Fig. 2a) and population imbalance (Fig. 2b) are practically constant, and the temperature (Fig. 2c) varies in a smooth linear way with the trap depth. In contrast, below the critical trap depth, the shape of the smaller cloud starts to deviate drastically from the Thomas-Fermi distribution of a normal gas, as quantified in Fig. 2d. This sudden increase in the standard deviation of a fit to a single-component fitting function is a standard way of identifying the BEC phase transition in a model-independent way².

Fig. 2e displays the fact that below the critical trap depth a new, third radius is required to

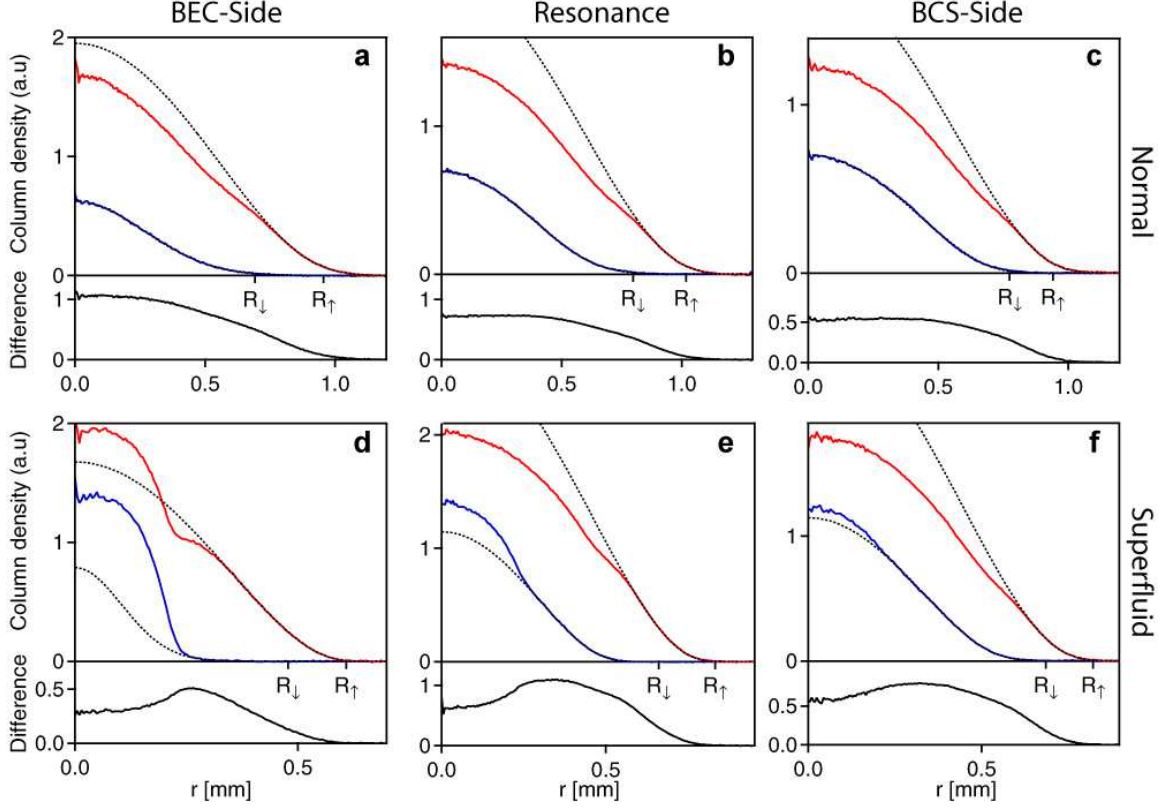


Figure 1: (Color online) Direct observation of the phase transition in a strongly interacting two-state mixture of fermions with imbalanced spin populations. Top **a-c** and bottom **d-f** rows show the normal and the superfluid state, respectively. Panels **a** and **d** were obtained in the BEC-regime (at 781 G), **b,e** on resonance ($B = 834$ G) and **c,f** on the BCS-side of the Feshbach resonance (at 853 G). The profiles represent the azimuthal average of the column density after 10 ms (BEC-side) or 11 ms (resonance and BCS-side) of expansion. The appearance of a dense central feature in the smaller component marks the onset of condensation. The condensate causes a clear depletion in the difference profiles (bottom of each panel). Both in the normal and in the superfluid state, interactions between the two spin states are manifest in the strong deformation of the larger component. The dashed lines show Thomas-Fermi fits to the wings of the column density. The radii R_{\uparrow} and R_{\downarrow} mark the Fermi radius of a ballistically expanding, non-interacting cloud with atom number N_{\uparrow} , N_{\downarrow} . The trap depth U , the atom numbers, the population imbalance $\delta = (N_{\uparrow} - N_{\downarrow})/(N_{\uparrow} + N_{\downarrow})$, the interaction parameter $1/k_F a$, the temperature T and the reduced temperature T/T_F were: **a**, $U = 4.8 \mu\text{K}$, $N_{\uparrow} = 1.8 \times 10^7$, $N_{\downarrow} = 2.6 \times 10^6$, $\delta = 75\%$, $1/k_F a = 0.42$, $T = 350$ nK, $T/T_F = 0.20$. **b**, $U = 3.2 \mu\text{K}$, $N_{\uparrow} = 1.8 \times 10^7$, $N_{\downarrow} = 4.2 \times 10^6$, $\delta = 63\%$, $1/k_F a = 0$ (resonance), $T = 260$ nK, $T/T_F = 0.15$. **c**, $U = 2.5 \mu\text{K}$, $N_{\uparrow} = 1.5 \times 10^7$, $N_{\downarrow} = 4.5 \times 10^6$, $\delta = 52\%$, $1/k_F a = -0.13$, $T = 190$ nK, $T/T_F = 0.12$. **d**, $U = 0.8 \mu\text{K}$, $N_{\uparrow} = 6.5 \times 10^6$, $N_{\downarrow} = 1.5 \times 10^6$, $\delta = 62\%$, $1/k_F a = 0.67$, $T = 50$ nK, $T/T_F \leq 0.05$. **e**, $U = 1.1 \mu\text{K}$, $N_{\uparrow} = 1.5 \times 10^7$, $N_{\downarrow} = 3.8 \times 10^6$, $\delta = 60\%$, $1/k_F a = 0$ (resonance), $T = 70$ nK, $T/T_F = 0.06$. **f**, $U = 1.2 \mu\text{K}$, $N_{\uparrow} = 1.3 \times 10^7$, $N_{\downarrow} = 4.4 \times 10^6$, $\delta = 50\%$, $1/k_F a = -0.15$, $T = 100$ nK, $T/T_F = 0.08$.

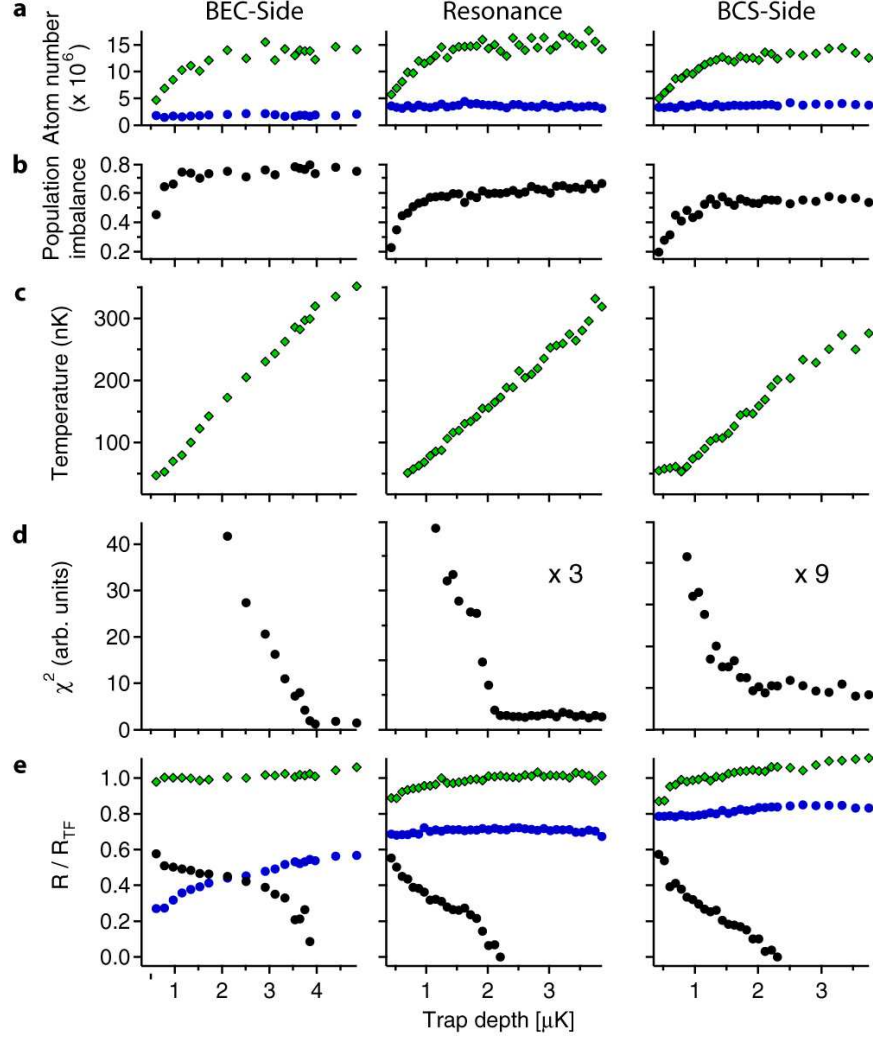


Figure 2: (Color online) Characterization of the phase transition. The data characterize the evolution of the fermion mixture as the cloud is evaporatively cooled by lowering the trap depth. The chosen magnetic fields are identical to those in Fig. 1. Data obtained from the majority (minority) cloud are shown as diamonds (circles). Shown are a) the atom number, b) population imbalance between the two spin states and c) the temperature of the spin mixture as determined from the non-interacting wings of the larger cloud's profile. d) A finite temperature Fermi-Dirac (for resonance and the BCS-side) or gaussian (for the BEC-side) distribution is fit to the minority cloud. The phase transition is marked by a sudden increase in χ^2 as the condensate starts to appear. e) Outer radii of the majority and minority cloud (for the minority cloud on the BEC-side: thermal cloud radius, all other cases: Thomas-Fermi radius) as well as the condensate radius, defined as the position of the "kink" in the minority profile (see Fig. 1). The radii of the majority and minority clouds are normalized to the Fermi-Radii $R_{\uparrow,\downarrow}$ of non-interacting atoms with atom number $N_{\uparrow,\downarrow}$, and adjusted for ballistic (hydrodynamic) expansion. Note that the imbalance decreases during evaporation because the larger majority cloud incurs stronger evaporative losses. For the data, three (BEC&Resonance) to five (BCS) independent measurements were averaged.

describe the two clouds. As we will see below, the appearance of this central feature coincides with the appearance of the fermion pair condensate in experiments involving the magnetic field ramp technique^{10–12}. It is this condensate which contains the superfluid vortices in^{8,12}. We are thus naturally led to interpret the central core as the condensate of fermion pairs, and the outer wings as the normal, uncondensed part of the cloud. This constitutes the first direct observation of the normal-to-superfluid phase transition in resonantly interacting Fermi gases on resonance and on the BCS-side (i.e. without a magnetic field sweep that so far cannot be quantitatively accounted for).

Already at high temperatures, above the phase transition, the larger cloud's profile is strongly deformed in the presence of the smaller cloud, a direct signature of interaction. Indeed, on resonance the cloud size of the minority component is significantly smaller than that of a non-interacting sample with the same number of atoms (see Fig. 2e). At the phase transition, the outer radii of the clouds do not change abruptly. This demonstrates that interactions, not superfluidity, are the main mechanism behind the reduced cloud size of an interacting Fermi gas.

On the BEC-side, the condensate is clearly visible in the larger cloud. On resonance, however, the condensate is not easily discernible in the larger component's profiles at the scale of Fig. 1. Nevertheless, we have found a very faint but reproducible trace of the condensate when analyzing the curvature of these column density profiles (see Fig. S1 in the Supplementary Information). On resonance and on the BCS-side, the onset of bimodality in the smaller cloud can be clearly observed for imbalances larger than $\sim 20\%$ (but below a certain critical imbalance, see below), for which the condensate is small compared to the minority cloud size. With increasing magnetic field on the BCS-side (i.e. with decreasing interaction strength), the bimodality becomes less pronounced and is not clearly discerned beyond 853 G ($1/k_F a < -0.15$).

Thermometry of strongly interacting Fermi gases has always been a major difficulty in experiments on strongly interacting fermions²². A thermometer can only be reliable if the working substance is not affected by the sample to be measured. In equal mixtures of fermions, the two overlapping atomic clouds are strongly interacting throughout. Temperatures determined from a non-interacting Thomas-Fermi fit to these clouds need calibration based on approximate theoretical calculations²². In addition, as will be reported elsewhere, we find that those fits do not describe the profiles of a partially superfluid Fermi gas as well as they do in the normal state, in agreement with theory^{14–17}. In the case of imbalanced mixtures, the wings of the larger component, where the spin down species are absent, are non-interacting and thus serve as a direct thermometer (see Fig. 2c). For an imbalance of $\delta = 75(3)\%$, we determine the critical temperature for the phase transition on the BEC-side at $1/k_F a = 0.46$ to be $T/T_F = 0.18(3)$ ($k_B T_F = \hbar\omega(3(N_\uparrow + N_\downarrow))^{1/3}$ - Fermi energy of a non-interacting, equal mixture with the same total number of fermions $N_\uparrow + N_\downarrow$, ω - geometric mean of the trapping frequencies). This corresponds to $T/T_{C,\downarrow} = 0.55(9)$ when comparing the temperature to the critical temperature $T_{C,\downarrow}$ for Bose-condensation in a non-interacting gas with N_\downarrow bosons. The reduction in the critical temperature is a direct consequence of strong repulsive interactions between the molecules. On resonance, at $\delta = 59(3)\%$, we find $T/T_F = 0.12(2)$, and on the BCS-side $1/k_F a = -0.14$ for $\delta = 53(3)\%$ we obtain $T/T_F = 0.11(2)$, where we have nor-

malized the temperature by the Fermi temperature of an equal mixture with the same number of atoms, $k_B T_F = \hbar\omega(3(N_\uparrow + N_\downarrow))^{1/3}$ ($\omega/2\pi$ - geometric mean of the trapping frequencies). These are the first directly measured and reliable temperatures for the superfluid transition in strongly interacting Fermi gases. They may serve as a checkpoint for theoretical models.

We note that the critical temperature will in general depend on the population imbalance. For example, for large enough imbalance on resonance or on the BCS-side, no condensate will form even at zero temperature¹², as we discuss below. Here, the critical temperature for superfluidity will be zero.

An important qualitative difference distinguishes the BEC-side from resonance: At the lowest temperatures on the BEC-side, the gas consists of only two parts: The superfluid core surrounded by a fully polarized degenerate Fermi gas of the excess species. On resonance and on the BCS-side, however, there exists a third region, a normal state in which both species are mixed. Several recent theories describe density profiles of imbalanced Fermi mixtures^{23–28}. Mean-field theories that neglect interactions in the normal cloud and between the normal and condensed cloud, are only in qualitative agreement with our results. Descriptions which exclude the mixed region or find superfluidity on resonance at all population imbalances are ruled out by our observations.

To elucidate the origin of the clear separation between condensate and normal components, we varied the population imbalance at our coldest temperatures and on resonance. Fig. 3b shows several resulting profiles after 11 ms expansion from the trap. For large imbalances, $\delta > 70\%$, the minority cloud is not bimodal and well fit by a (unconstrained) Thomas-Fermi profile. At a critical imbalance of $\delta \approx 70\%$, the condensate appears and then grows further as the imbalance is reduced (for the cloud radii see Fig. S2 in the Supplementary Information).

To characterize the appearance of the condensate for imbalances around $\delta = 70\%$, a Thomas-Fermi profile is fit to the wings of the minority cloud. The fraction of atoms not contained in this fit is a measure of the condensate fraction (see Fig. 3). We find a critical imbalance of $\delta_c = 70(5)\%$ above which the condensate disappears. This agrees with our previous work¹², where we employed a rapid ramp method to the BEC-side to extract the condensate fraction. We observed the quantum phase transition from the superfluid to the normal state as a critical population imbalance of $\delta_c = 70\%$ was exceeded. This strongly suggests that the bimodality observed here directly in the minority component and the bimodality observed in molecular clouds after a magnetic field sweep are signatures of the same phase transition.

The transition at δ_c is known as the Clogston limit of superfluidity^{12,29} and occurs when the chemical potential difference $\delta\mu$ becomes larger than the (local) superfluid gap $\Delta(\mathbf{r})$ (see Supplementary Information). Here we present a simple picture for the character of this phase transition in a harmonic trap. Thomas-Fermi-fits for the normal clouds beyond δ_c allow a simple estimate of the central 3D-density of the gas (with an estimated accuracy of 20% for the relative density difference), shown in the inset of Fig. 3. For large imbalances, we find that the 3D-densities differ significantly, as is expected for two weakly interacting Fermi clouds. As the imbalance is re-

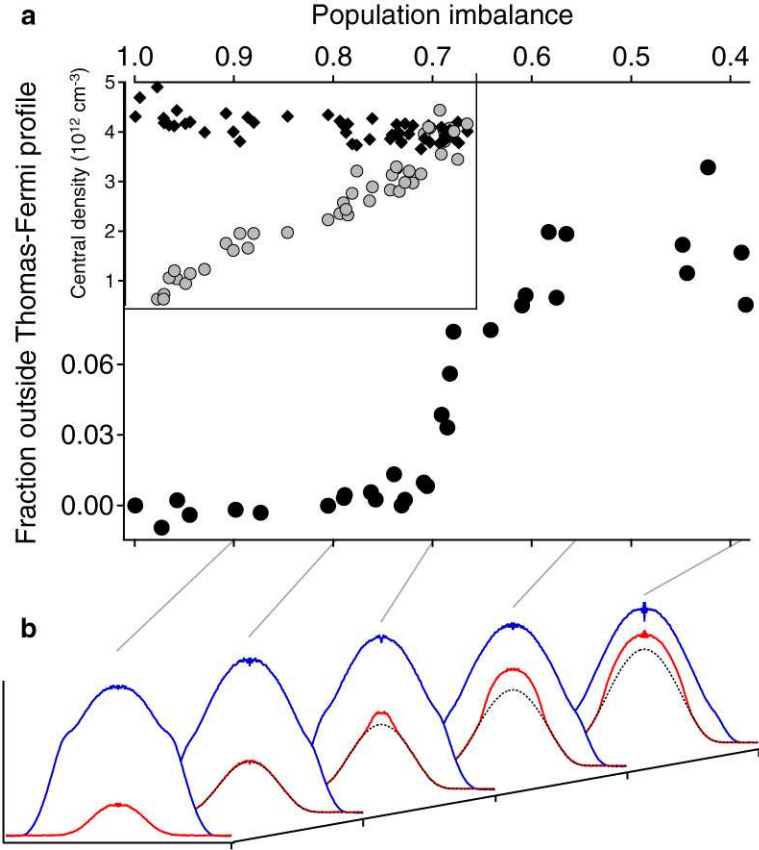


Figure 3: (Color online) Quantum phase transition to superfluidity for decreasing population imbalance. **a**, The "condensate fraction" of excess minority atoms, not contained in the Thomas-Fermi fit, versus population imbalance on resonance. **b**, Column density profiles, azimuthally averaged, for varying population imbalance. The condensate is clearly visible in the minority component as the dense central feature on top of the normal background (finite-temperature Thomas-Fermi fit, dotted lines). Below the critical imbalance $\delta_c = 70\%$, the condensate starts to form. The inset in **a** shows the central densities of the larger (black diamonds) and smaller (grey circles) cloud in the normal state above δ_c . This demonstrates that here the central densities are unequal, suppressing superfluidity. The densities were calculated from the central optical density and the fitted size of the clouds, assuming local density approximation and adjusting for ballistic (hydrodynamic) expansion of the outer radii of majority (minority) clouds. The data-points for the condensate fraction show the average of several independent measurements.

duced towards the critical δ_c , the central densities approach each other and become approximately equal around δ_c . This is a direct consequence of strong interactions in the normal state. In a non-interacting Fermi mixture with an imbalance of δ_c , the central densities would differ by a factor of 2.4.

This observation now offers an intriguing insight into the nature of a fermionic superfluid on resonance or on the BCS-side. Already in the normal state above T_C or beyond $\delta = \delta_c$, interactions between the two spin states are strong. Indeed, this is directly seen in the deformation of the majority cloud due to the presence of the minority species (see Figs. 1, 3). However, here these interactions are not strong enough to let the central densities of the two clouds become comparable. At the critical imbalance the Clogston criterion $\delta\mu = \Delta(0)$ is fulfilled in the center of the trap. For smaller imbalance, a central superfluid region can form, the condensate. Its borders are defined by $\delta\mu < \Delta(r)$. The simple density estimate in Fig. 3 suggests that this region will be of equal densities, although more refined techniques to measure small density differences have to be developed to finally conclude on this question. Outside the superfluid region there is still a normal state with unequal densities of minority and majority components. The discontinuity in the clouds' densities at the normal-to-superfluid phase boundary gives rise to the visible kink in the column density profiles. Such a density discontinuity is characteristic for a first-order phase transition.

Interestingly, most of the “work” to build the superfluid state is already done in the normal component by decreasing the density difference. Consequently, the critical population difference to form the *superfluid* is largely determined by the interactions in the *normal* gas.

In conclusion, we have observed the normal-to-superfluid phase transition through the direct observation of condensation in an imbalanced Fermi mixture, on the BEC-side, on the BCS-side and right on the Feshbach resonance. Unequal mixtures offer a direct method of thermometry by analyzing the non-interacting wings of the majority species. Strong interactions are already visible in the normal cloud as marked deformations of the majority profile. It is these interactions in the normal gas which squeeze the two components and eventually, at the critical imbalance, let them reach almost equal densities in the center, aiding the formation of the superfluid. Our method of direct detection of the condensate is a powerful new tool to characterize the superfluid phase transition. At the current level of precision, the appearance of a condensate after magnetic field sweeps and the direct observation of the central dense core occur together and indicate the normal-to-superfluid phase transition. An intriguing question is whether further phases are possible, including a more exotic superfluid state with unequal densities. Several theories predict that the FFLO-state, a superfluid state with oscillating order parameter, should be present for imbalanced spin populations^{24,30}.

Methods

Our experimental setup is described in previous publications^{8,12}. A spin-polarized cloud of ^6Li fermions is cooled to degeneracy using a combination of laser cooling and sympathetic cooling with sodium atoms in a magnetic trap. After transfer into an optical trap, a variable spin mixture of

the lowest two hyperfine states, labelled $|\uparrow\rangle$ and $|\downarrow\rangle$ is prepared at a magnetic bias field of 875 G. Interactions between the two spin states can be freely tuned via a 300 G wide Feshbach resonance located at $B_0 = 834$ G. At fields below B_0 , two-body physics supports a stable molecular bound state (BEC-side), while at higher fields (BCS-side), no such bound state exists for two isolated atoms. Our trap combines a magnetic saddle potential with a weakly focused (waist $w \approx 120 \mu\text{m}$) infrared laser beam (wavelength $\lambda = 1064$ nm), leading to a harmonic axial confinement with oscillation frequency of $\nu_z = 22.8(0.2)$ Hz and a gaussian radial potential with variable trapping frequency ν_r in the central harmonic region. The trap depth U is related to ν_r and ν_z via

$$U = \frac{1}{4} m (2\pi\nu_r)^2 w^2 \left(1 - \frac{\nu_z^2}{2\nu_r^2} \ln \left(\frac{2(\nu_r^2 + \nu_z^2/2)}{\nu_z^2} \right) \right).$$

The initial degeneracy of the spin-mixture is about $T/T_F \approx 0.3$. The strongly interacting gas is further cooled by decreasing the laser power of the optical trap in several seconds and evaporating the most energetic particles. During the first few seconds, the magnetic field is adiabatically ramped to a chosen final field in the resonance region where the last stage of the evaporation (shown in Fig. 2) takes place. For detection, the optical trap is switched off and the gas expands in the remaining magnetic saddle point potential. After a variable time-of-flight an absorption image of atoms either in state $|\uparrow\rangle$ or $|\downarrow\rangle$ is taken along the axial direction of the trap (the direction of the optical trapping beam). The cloud's radial symmetry allows for azimuthal averaging of the resulting column densities, leading to low-noise profiles¹².

For preparing clouds at the coldest temperatures (as shown in Fig. 3) with varying population imbalance, the spin mixture is evaporated down to a trap depth of $1 \mu\text{K}$ over several seconds on resonance, after which the trap depth is increased again to $1.4 \mu\text{K}$ for more harmonic confinement (trap frequencies: $\nu_r = 115(10)$ Hz and $\nu_z = 22.8(0.2)$ Hz). The temperature of the gas is determined to be $T/T_F \leq 0.06$ for all $\delta > 15\%$, and appeared to smoothly raise to $T/T_F = 0.11$ for an equal mixture, although thermometry in the interacting wings is problematic. The total atom number was 1.5×10^7 and constant to within 15% for all values of δ .

The error in the critical temperature T_C/T_F for the phase transition is dominated by the uncertainty in the atom number entering the determination of T_F , which we estimate to be 30%¹². For T_F we use the harmonic approximation for the radially gaussian trapping potential, with the measured trapping frequencies reflecting the average curvature of the gaussian potential. The phase transition is observed above $U = 2 \mu\text{K}$, where anharmonicities contribute only 3% to the error in T_F . Note that anharmonicities do not affect the temperature measurement performed on the majority wings: Ballistic expansion of non-interacting atoms reveals their momentum distribution, regardless of the shape of the trap.

1. Anderson, M. H., Ensher, J. R., Matthews, M. R., Wieman, C. E. & Cornell, E. A. Observation of Bose-Einstein Condensation in a Dilute Atomic Vapor. *Science* **269**, 198–201 (1995).

2. Davis, K. B. *et al.* Bose-Einstein Condensation in a Gas of Sodium Atoms. *Phys. Rev. Lett.* **75**, 3969–3973 (1995).
3. Greiner, M., Regal, C. A. & Jin, D. S. Emergence of a molecular Bose-Einstein condensate from a Fermi gas. *Nature* **426**, 537 (2003).
4. Zwierlein, M. W. *et al.* Observation of Bose-Einstein Condensation of Molecules. *Phys. Rev. Lett.* **91**, 250401 (2003).
5. Bartenstein, M. *et al.* Crossover from a Molecular Bose-Einstein Condensate to a Degenerate Fermi Gas. *Phys. Rev. Lett.* **92**, 120401 (2004).
6. Bourdel, T. *et al.* Experimental Study of the BEC-BCS Crossover Region in Lithium 6. *Phys. Rev. Lett.* **93**, 050401 (2004).
7. Partridge, G. B., Strecker, K. E., Kamar, R. I., Jack, M. W. & Hulet, R. G. Molecular Probe of Pairing in the BEC-BCS Crossover. *Phys. Rev. Lett.* **95**, 020404 (2005).
8. Zwierlein, M. W., Abo-Shaeer, J. R., Schirotzek, A., Schunck, C. H. & Ketterle, W. Vortices and superfluidity in a strongly interacting Fermi gas. *Nature* **435**, 1047–1051 (2005).
9. Regal, C. A., Greiner, M. & Jin, D. S. Observation of Resonance Condensation of Fermionic Atom Pairs. *Phys. Rev. Lett.* **92**, 040403 (2004).
10. Zwierlein, M. W. *et al.* Condensation of Pairs of Fermionic Atoms near a Feshbach Resonance. *Phys. Rev. Lett.* **92**, 120403 (2004).
11. Zwierlein, M. W., Schunck, C. H., Stan, C. A., Raupach, S. M. F. & Ketterle, W. Formation Dynamics of a Fermion Pair Condensate. *Phys. Rev. Lett.* **94**, 180401 (2005).
12. Zwierlein, M. W., Schirotzek, A., Schunck, C. H. & Ketterle, W. Fermionic Superfluidity with Imbalanced Spin Populations. *Science* **311**, 492–496 (2006). Published online 21 December 2005 (10.1126/science.1122318).
13. Partridge, G. B., Li, W., Kamar, R. I., a. Liao, Y. & Hulet, R. G. Pairing and Phase Separation in a Polarized Fermi Gas. *Science* **311**, 503 (2006). Published online 21 December 2005 (10.1126/science.1122876).
14. Chiofalo, M. L., Kokkelmans, S. J. J. M. F., Milstein, J. N. & Holland, M. J. Signatures of Resonance Superfluidity in a Quantum Fermi Gas. *Phys. Rev. Lett.* **88**, 090402 (2002).
15. Ho, T.-L. Universal Thermodynamics of Degenerate Quantum Gases in the Unitarity Limit. *Phys. Rev. Lett.* **92**, 090402 (2004).
16. Perali, A., Pieri, P., Pisani, L. & Strinati, G. C. BCS-BEC Crossover at Finite Temperature for Superfluid Trapped Fermi Atoms. *Phys. Rev. Lett.* **92**, 220404 (2004).

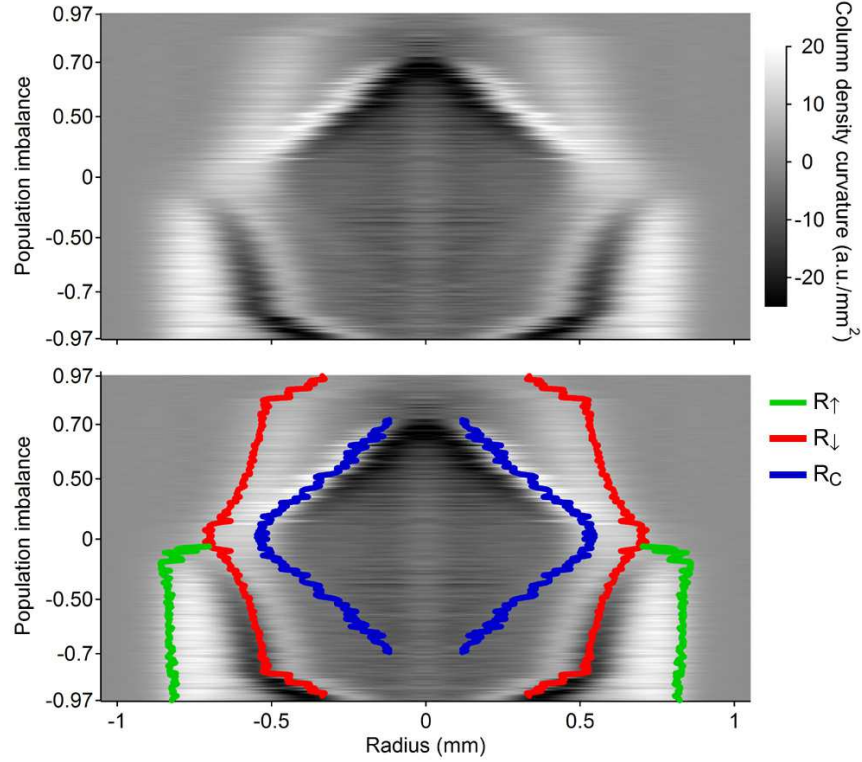
17. Stajic, J., Chen, Q. & Levin, K. Density Profiles of Strongly Interacting Trapped Fermi Gases. *Phys. Rev. Lett.* **94**, 060401 (2005).
18. Diener, R. B. & Ho, T.-L. Projecting Fermion Pair Condensates into Molecular Condensates. Preprint at <<http://arxiv.org/cond-mat/0404517>> (2004).
19. Perali, A., Pieri, P. & Strinati, G. C. Extracting the Condensate Density from Projection Experiments with Fermi Gases. *Phys. Rev. Lett.* **95**, 010407 (2005).
20. Altman, E. & Vishwanath, A. Dynamic Projection on Feshbach Molecules: A Probe of Pairing and Phase Fluctuations. *Phys. Rev. Lett.* **95**, 110404 (2005).
21. Chen, Q., Regal, C. A., Greiner, M., Jin, D. S. & Levin, K. Understanding the superfluid phase diagram in trapped fermi gases. *Phys. Rev. A* **73**, 041603 (2006).
22. Kinast, J. *et al.* Heat Capacity of a Strongly-Interacting Fermi Gas. *Science* **307**, 1296–1299 (2005).
23. Pieri, P. & Strinati, G. C. Trapped Fermions With Density Imbalance in the Bose-Einstein Condensate Limit. *Phys. Rev. Lett.* **96**, 150404 (2006).
24. Kinnunen, J., Jensen, L. M. & Törmä, P. Strongly Interacting Fermi Gases with Density Imbalance. *Phys. Rev. Lett.* **96**, 110403 (2006).
25. De Silva, T. N. & Mueller, E. J. Density profiles of an imbalance trapped Fermi gas near a Feshbach resonance Preprint at <<http://arxiv.org/cond-mat/0601314>> (2006).
26. Yi, W. & Duan, L.-M. Trapped Fermions across a Feshbach resonance with population imbalance. *Phys. Rev. A* **73**, 031604(R) (2006).
27. Chevy, F. Density Profile of a Trapped Strongly Interacting Fermi Gas with Unbalanced Spin Populations. *Phys. Rev. Lett.* **96**, 130401 (2006).
28. Haque, M. & Stoof, H. T. C. Pairing of a trapped resonantly-interacting fermion mixture with unequal spin populations. Preprint at <<http://arxiv.org/cond-mat/0601321>> (2006).
29. Clogston, A. M. Upper limit for the critical field in hard superconductors. *Phys. Rev. Lett.* **9**, 266 (1962).
30. Mizushima, T., Machida, K. & Ichioka, M. Direct imaging of spatially modulated superfluid phases in atomic fermion systems. *Phys. Rev. Lett.* **94**, 060404 (2005).

Acknowledgements We would like to thank the participants of the Aspen winter conference on strongly interacting fermions for stimulating discussions. This work was supported by the NSF, ONR, and NASA.

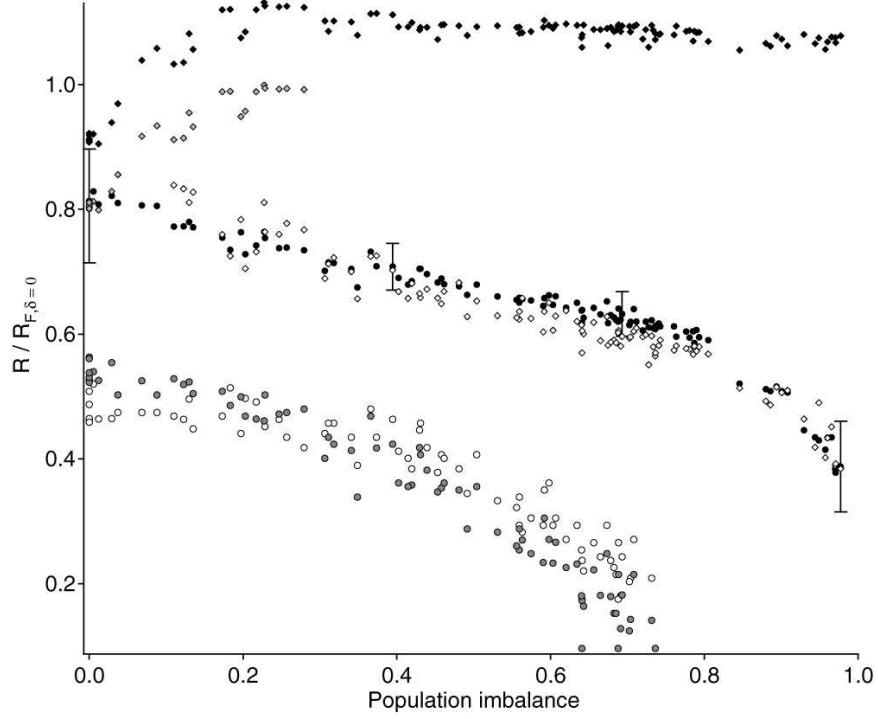
Author Information Correspondence and requests for materials should be addressed to M. W. Z. (email: zwierlei@mit.edu).

Supplementary Information

Supplementary Figures



Supplementary Figure 4: (Color online) Signatures of the condensate on resonance in the spatial profiles. The curvature of the observed column density is encoded in shades of gray with white (black) corresponding to positive (negative) curvature. The outer radii of the two components and the condensate radius are shown as an overlay in the lower panel. As a direct consequence of strong interactions, the minority component causes a pronounced bulge in the majority density that is reflected in the rapid variation of the profile's curvature. The condensate is clearly visible in the minority component ($\delta > 0$), but also leaves a faint trace in the majority component ($\delta < 0$). The image was composed out of 216 individual azimuthally averaged column density profiles, smoothed to reduce technical noise. Data close to the cloud's center suffer from larger noise due to the lower number of averaged points. The central feature of about $50\mu\text{m}$ width is an artefact of smoothing in this region of increased noise.



Supplementary Figure 5: Outer radii of the two cloud profiles and condensate radius versus population imbalance. Data obtained from the majority (minority) cloud are shown as diamonds (circles). The outer radii of the clouds (black) are determined from Thomas-Fermi fits to the profiles' wings, where the results of a zero-temperature and a finite temperature fit were averaged. For the minority cloud, the representative error bars indicate the difference between these two results. The position of the "bulge" in the majority profile (white diamonds) naturally follows the outer minority radius. The condensate radius is defined as the position of the "kink" in the minority profiles. It was obtained by a) fitting an increasing portion of the minority wings until a significant increase in χ^2 was observed (grey circles), and b) the position of the minimum in the profile's derivative (white circles). All sizes are scaled by the Fermi-radius of a non-interacting equal mixture. The minority radii were adjusted for the observed hydrodynamic expansion (expansion factor 11.0). The non-interacting wings of the majority cloud expand ballistically (expansion factor 9.7), as long as they are found a factor $11/9.7 = 1.13$ further out than the minority radius. For small imbalances ($\delta < 20\%$), also the majority wing's expansion will be affected by collisions. The grey diamonds give the majority cloud's outer radius if hydrodynamic expansion is assumed.

Supplementary Methods

Hydrodynamic vs. ballistic expansion

A non-interacting cloud of atoms simply expands ballistically from a trap. However, strongly interacting equal Fermi mixtures, above and below the phase transition, are collisionally dense and therefore expand according to hydrodynamic scaling laws¹⁻³. These scaling laws only depend on the equation of state of the gas, $\epsilon \propto n^\gamma$, with $\gamma = 1$ for the BEC-side, $\gamma = 2/3$ for resonance (a direct consequence of unitarity) and $\gamma = 2/3$ for the BCS-side, away from resonance. In an unequal spin mixture of fermions, the expansion does not follow a simple scaling law. The minority cloud is always in contact with majority atoms and thus strongly interacting throughout the expansion, which is therefore hydrodynamic. The excess atoms in the wings of the larger cloud are non-interacting and will expand ballistically, as we have checked experimentally. The absorption images after expansion are taken along the axial direction of the trap (the direction of the optical trapping beam). In order to compare the expanded cloud sizes to the in-trap Fermi radii of non-interacting clouds (see Fig. 2 and Fig. S2 above) we scale the majority cloud with the ballistic factor for the radial direction

$$\sqrt{\cosh^2\left(2\pi\nu_z t/\sqrt{2}\right) + (\sqrt{2}\nu_r/\nu_z)^2 \sinh^2\left(2\pi\nu_z t/\sqrt{2}\right)},$$

where t is the expansion time and $\nu_z/\sqrt{2}$ gives the radial anti-trapping curvature of the magnetic saddle-point potential. The scaling factor for the hydrodynamic expansion of an equal mixture is given by the solution to a differential equation^{2,3}. A priori, the minority cloud in unequal mixtures could expand with a different scaling, since the equation of state now depends on *two* densities. However, by imaging the cloud in trap and at different times during expansion, we found that the minority cloud's expansion is very well described by the scaling law for an equal mixture. In particular, the aspect ratio of the minority cloud did not change as a function of population imbalance (within our experimental error of 5%), and was equal to that of a balanced mixture.

For the data on resonance in Figs. 3, S1 and S2, which were obtained after 11 ms expansion out of a trap with radial (axial) frequency of $\nu_r = 113(10)$ Hz ($\nu_z = 22.8(0.2)$ Hz), the ballistic (hydrodynamic) expansion factor for the radial direction is 9.7 (11.0).

Supplementary Discussion

Signature of the condensate

Fig. S1 demonstrates that on resonance, the condensate is visible not only in the minority component, but also in the larger cloud as a small change in the profile's curvature. In the condensate region, the majority profile is slightly depleted when compared to the shape of a normal Fermi cloud. This effect is still significant on the BCS-side (see Fig. 1): Although here, the condensate is less visible in the smaller component than on resonance, the larger cloud's central depletion still produces a clear dip in the difference profile.

Radii in the unequal Fermi mixture

Fig. S2 shows the outer radii of the majority and minority cloud, together with the condensate radius (on resonance, for the deepest evaporation compatible with constant total atom number versus imbalance). As was the case for the phase transition at finite temperature, the outer cloud sizes change smoothly with imbalance. No drastic change is seen at the critical population imbalance. The radii are obtained by fitting the profiles' wings to the Thomas-Fermi expression for the radial column density $n(r)$:

$$n(r) = n_0 \frac{\text{Li}_2\left(-\lambda^{1-r^2/R^2}\right)}{\text{Li}_2(-\lambda)},$$

with the central column density n_0 , the fugacity λ and the Thomas-Fermi radius R as the free parameters. $\text{Li}_2(x)$ is the Dilogarithm. The zero-temperature expression reduces to $n(r) = n_0(1 - r^2/R^2)^2$.

Lower and upper bounds for the critical chemical potential difference at δ_c

For the clouds at the critical imbalance δ_c , we now want to extract a lower and upper bound for the difference in chemical potentials $\delta\mu_c$ of the majority and minority component. This difference allows us to conclude that BCS-type superfluidity with imbalanced densities is not possible.

The chemical potential difference $\delta\mu \equiv 2h = (\mu_\uparrow - \mu_\downarrow)$ measures the energy cost, relative to $\mu = (\mu_\uparrow + \mu_\downarrow)/2$, to add a particle to the cloud of excess fermions. Δ , the pairing gap, is the energy cost for this additional majority particle to enter the superfluid. Both the critical temperature T_C and the critical chemical potential difference $\delta\mu_c$ provide a measure of the superfluid gap: The superfluid can be either destroyed by raising the temperature or by increasing the population imbalance. If $h_c \equiv \delta\mu_c/2 < \Delta$, excess atoms will always stay outside the superfluid, in the phase separated normal state. For $h_c > \Delta$, excess atoms can enter the superfluid for $h_c > h > \Delta$. Hence, superfluidity with unequal densities, if allowed via $h_c > \Delta$, would be favored at large population imbalance, contrary to the interpretation in ⁴, where such a state was proposed for small population imbalance. A recent Monte-Carlo calculation ⁵ for the Clogston limit on resonance gives $h_c = 1.00(5)\Delta = 0.50(5)E_F$ and can thus not decide on the question of superfluidity with imbalanced densities.

We can attempt to extract the chemical potential from the cloud sizes $R_{\uparrow,\downarrow}$ - taking into account hydrodynamic expansion for the minority cloud and ballistic expansion for the excess fermions. For the majority cloud, we find $\mu_{c,\uparrow} = 1/2m\omega_r^2 R_{\uparrow}^2 = 1.21(6)E_F$. For the minority cloud, we find $1/2m\omega_r^2 R_{\downarrow}^2 = 0.39(10)E_F$. Throughout the smaller cloud, minority atoms are always strongly attracted by majority atoms. This strong attractive interaction likely reduces their chemical potential from the above upper limit. The difference of the chemical potentials $\delta\mu_c \equiv 2h_c$ is thus given by $h_c = (\mu_{c,\uparrow} - \mu_{c,\downarrow})/2 \geq 0.41(6)E_F = 0.51\mu$, our lower bound. Another condition on h_c concerns whether the normal state can be mixed, $h_c < \mu$, (minority and majority atoms in the same spatial region) or whether the normal state is always completely polarized $h_c > \mu$. Our

observation of the mixed region in Fig. 1 immediately results in $h_c < \mu$, the upper bound.

On resonance, $\Delta = 1.16\mu$ in BCS-theory, while a recent Monte-Carlo study ⁵ obtains $\Delta = 1.2\mu$. If $\Delta > \mu$ holds true, our finding of the upper bound on h_c would imply $h_c < \Delta$ and hence would exclude a superfluid with unequal spin densities (at least on the basis of BCS-theory, see ⁶ for a recent suggestion which goes beyond BCS).

Supplementary Notes

1. O'Hara, K. M., Hemmer, S. L., Gehm, M. E., Granade, S. R. & Thomas, J. E. Observation of a strongly interacting degenerate fermi gas of atoms. *Science* **298**, 2179 (2002).
2. Menotti, C., Pedri, P. & Stringari, S. Expansion of an Interacting Fermi gas. *Phys. Rev. Lett.* **89**, 250402 (2002).
3. Castin, Y. Exact scaling transform for a unitary quantum gas in a time dependent harmonic potential. *Comptes Rendus Physique* **5**, 407–410 (2004).
4. Partridge, G. B., Li, W., Kamar, R. I., a. Liao, Y. & Hulet, R. G. Pairing and Phase Separation in a Polarized Fermi Gas. *Science* **311**, 503 (2006). Published online 21 December 2005 (10.1126/science.1122876).
5. Carlson, J. & Reddy, S. Asymmetric Two-Component Fermion Systems in Strong Coupling. *Phys. Rev. Lett.* **95**, 060401 (2005).
6. Ho, T.-L. & Zhai, H. Homogeneous Fermion Superfluid with Unequal Spin Populations. Preprint at <<http://arxiv.org/cond-mat/0602568>> (2006).